Journal of the Korean Nuclear Society
Volume 32, Number 1, pp.34~45, February 2000

The Effect of Coolant Boiling on the Molten Metal Pool Heat Transfer with Local Solidification

Jae-Seon Cho, Kune Y. Suh and Chang-Hyun Chung
Seoul National University
56-1 Shinrim-dong, Kwanak-gu, Seoul, 151-742, Korea
dynamics@gong.snu.ac.kr

Rae-Joon Park and Sang-Baik Kim
Korea Atomic Energy Research Institute
150 Dukjin-dong, Yusong-gu, Taejon, 305-353, Korea
(Received June 7, 1999)

Abstract

This study is concerned with the experimental test and numerical analysis of the heat transfer and solidification of the molten metal pool with overlying coolant with boiling. In the test, the metal pool is heated from the bottom surface and coolant is injected onto the molten metal pool. Experiments were performed by changing the test section bottom surface temperature of the metal layer and the coolant injection rate. The two-phase boiling coolant experimental results are compared against the dry test data without coolant or solidification of the molten metal pool, and against the crust formation experiment with subcooled coolant. Also, a numerical analysis is performed to check on the measured data. The numerical program is developed using the enthalpy method, the finite volume method and the SIMPLER algorithm. The experimental results of the heat transfer show general agreement with the calculated values. The present empirical test and numerical results of the heat transfer on the molten metal pool are apparently higher than those without coolant boiling. This is probably because this experiment was performed in concurrence of solidification in the molten metal pool and the rapid boiling of the coolant. The other experiments were performed without coolant boiling and the correlation was developed for the pure molten metal without phase change.

Key Words : severe accident, molten metal pool, natural convection heat transfer, solidification, boiling coolant, Nu, Ra

1. Introduction

During a hypothetical severe accident in nuclear power plants, stratified fluid layers may exist in the form of a high temperature molten debris pool and water coolant in the lower plenum of the reactor vessel or in the reactor cavity[1-3]. Also, the molten debris pool may be stratified into a

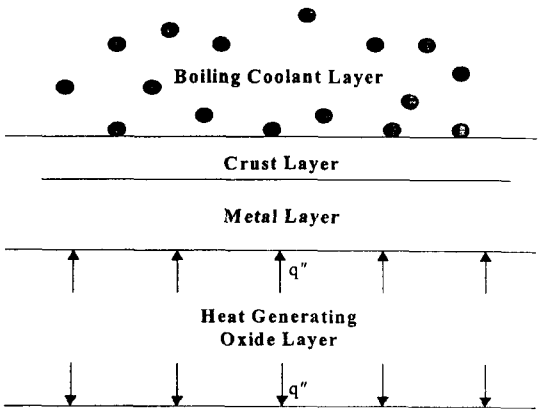

Fig. 1. Sketch of the Molten Debris and Coolant Layers

metal layer and an oxide layer on account of their density difference[4-6]. As shown in Fig. 1, a molten metal layer is located in the upper region and cooled by overlying coolant which may undergo boiling. As a result, the crust, which is a solidified layer of the molten pool, may form at the top. Heat transfer is accomplished by a conjugate mechanism consisting of natural convection in the molten metal pool, conduction through the crust layer and convective boiling heat transfer to the coolant [7, 8].

The heat transfer and solidification processes in the molten metal pool are of fundamental importance in the severe accident progression. A number of experimental and theoretical investigations were performed to understand the solidification and the change of heat transfer rate of the debris pool, which greatly affects the accident progression.

Experimental and numerical studies were performed to investigate the crust formation and heat transfer characteristics of the molten metal pool with overlying coolant with boiling. Tests were conducted under the condition of bottom surface heating in the test section and forced convection of the coolant being injected onto the molten metal pool. The test parameters spanned the heated bottom surface temperature of the molten metal pool, the coolant injection rate and the coolant injection temperature. Numerical analyses were performed in the two-dimensional rectangular domain of the molten metal pool.

2. Experimental Setup and Test Procedure

Fig. 2 shows a schematic diagram of the test section. The inner rectangular test section is 25cm long, 25cm wide, and 35cm high. The test section is made of 10mm thick STS304 stainless steel. The molten metal and coolant layers are 20cm and 15cm deep, respectively. A 20kW heater is installed in the bottom horizontal plate of the test section. The bottom heating surface temperature is monitored using a thermometer. The bottom heating surface temperature is controlled to maintain uniformity by utilizing a heater controller. The viewports are installed using a quartz glass at the front and back of the test section. Four sides of the test section are insulated with a 4cm thick Fiberfrax material to minimize heat loss. A digital pump is installed to deliver a uniform mass flow of the coolant onto the molten metal pool. The melting pot is equipped with an 8kW heater to melt the metal. The translating tube, which is connected from the melting pot to the test section, is wrapped so as to prevent solidification of the molten metal using a heating tape. The temperature distribution inside the test section is measured using 85 thermocouples of 0.5mm diameter, which are placed in five arrays of thermocouple bundles located at the one-fourth, one-half and three-fourth positions of the length and width of the test section. The thermocouple is of T-type(copper-constantan) and aligned in

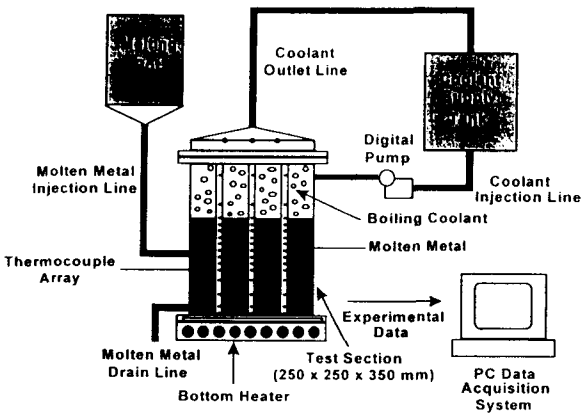

Fig. 2. Schematic Diagram of the Experimental Setup

the vertical direction in a bundle. Fifteen of the seventeen thermocouples are immersed into the metal layer and two thermocouples are located in the coolant layer. The data acquisition system(DAS) consists of an IBM PC using the Visual Designer, which displayed and stored all of the thermocouple readings. The simulant molten pool material is tin (Sn) with the melting temperature of 232℃. Tin has no toxicity and has a low corrosion effect on other materials. The solidification shrinkage of tin is estimated to be 2.7%. Demineralized water is used as the working coolant.

The test parameters are the bottom surface temperature ranging from 253℃ to 266℃, the injection coolant mass flow rate, with a range of 0.5kg/min to 2.5kg/min, and the injection coolant temperature ranging from 82℃ to 95℃. Tests were performed at atmospheric pressure.

First, the metal is molten in the melting pot and injected into the test section. The metal is maintained as liquid in the test section whose bottom surface is electrically heated. To avoid any potential steam explosion when the coolant is injected, the coolant is heated up to nearly the boiling temperature. Next, the coolant is injected onto the molten metal in the test section at the preset mass flow rate. Then, the upper region of the molten metal layer starts to solidify and the solidified layer thickens with the lapse of time. The boiling coolant is transported to the quench tank from the test section. The vapor is condensed in the quench tank and transported to the coolant supply tank. The coolant is recirculated in a closed loop until a steady-state condition is achieved. A steady state condition is assumed when the crust thickness of the metal layer stabilizes with time. After the steady state is accomplished, the PC data acquisition system records the temperature data of metal and coolant layers.

3. Numerical Analysis

3.1. Governing Equations

An algorithm is developed to analyze problems of solidifying liquid due to heat transfer. Heat transfer in a fluid is governed by the basic equations expressing conservation of mass, momentum and energy. When a phase change from liquid to solid occurs, any accompanying change of density is neglected and the velocities in the solid are zeroed.

To analyze the solidification and heat transfer of the molten metal, a Stefan problem is formulated. In the classical Stefan formulation, the energy equation can be described by a pair of heat conduction equations for the solid and liquid regions. Also, the boundary condition is needed at the phase change(i.e. the solid-liquid interface). In this study, the enthalpy formulation is adopted for the energy equation[9]. This approach removes the requirement to satisfy conditions at the beginning of the phase change, but zero velocity conditions are needed as liquid turns to solid. The governing equations for the analytical model are expressed in the two-dimensional Cartesian coordinates as:

Continuity Equation:

$$\frac{\partial \rho}{\partial t} + \frac{\partial}{\partial x}(\rho v_x) + \frac{\partial}{\partial y}(\rho v_y) = 0 \quad (1)$$

Momentum Equation:

$$\frac{\partial(\rho v_x)}{\partial t} + v_x \frac{\partial(\rho v_x)}{\partial x} + v_y \frac{\partial(\rho v_x)}{\partial y} = -\frac{\partial p}{\partial x} + \mu\left(\frac{\partial^2 v_x}{\partial x^2} + \frac{\partial^2 v_x}{\partial y^2}\right) + A v_x \quad (2)$$

$$\frac{\partial(\rho v_y)}{\partial t} + v_x \frac{\partial(\rho v_y)}{\partial x} + v_y \frac{\partial(\rho v_y)}{\partial y} = \frac{\partial p}{\partial y} + \mu\left(\frac{\partial^2 v_y}{\partial x^2} + \frac{\partial^2 v_y}{\partial y^2}\right) + A v_y + \frac{\rho_{ref} g \beta (h - h_{ref})}{c_p} \quad (3)$$

Energy Equation:

$$\frac{\partial(\rho h)}{\partial t} + v_x \frac{\partial(\rho h)}{\partial x} + v_y \frac{\partial(\rho h)}{\partial y} = \frac{k}{c_p}\left(\frac{\partial^2 h}{\partial x^2} + \frac{\partial^2 h}{\partial y^2}\right) - \frac{\partial(\rho \Delta H)}{\partial t} \quad (4)$$

where

$$A = \begin{cases} 0 & T \geq T_m \\ -1.6 \times 10^6 & T < T_m \end{cases} \quad (5)$$

$$\Delta H = \begin{cases} L & T \geq T_m \\ 0 & T < T_m \end{cases} \quad (6)$$

g : gravitational acceleration
c_p : specific heat at constant pressure
k : thermal conductivity
μ : dynamic viscosity
h : enthalpy
h_{ref} : enthalpy at T_{ref}
L : latent heat of fusion
p : pressure
T_m : melting temperature
T_{ref} : reference temperature
v_x : x-directional velocity
v_y : y-directional velocity
β : thermal expansion coefficient
ρ : density
ρ_{ref} : density at T_{ref}

The last term on the right side of equation (3) is a buoyancy term used to induce the natural convection in the molten pool. It is considered that a pure material does not have a mushy region and thus solidifies simply at temperature $T = T_m$. The term A is used to modify the velocity that approaches zero in the crust region [10].

3.2. Numerical Modelling

The numerical calculation is carried out with modification of the numerical methods presented by Patankar.11 For the governing equations shown in the preceding section, the general equation can be established in the form:

$$\frac{\partial}{\partial t}(\rho \phi) + div(\rho \vec{v} \phi) = div(\Gamma \, grad \, \phi) + S \quad (7)$$

where

$\vec{v}$: velocity vector
Γ : material properties such as μ, k/c_p

The Four terms in the above are an unsteady term and the convection term on the left side, and the diffusion term and the source term on the right side. The dependent variable ϕ stands for a variety of quantities such as the velocity component or the enthalpy. Accordingly, for each of these variables, an appropriate meaning will have to be given to the diffusion coefficient Γ and the source term S. Table I presents the corresponding values in the governing equations.

The numerical technique used here is the finite volume method and the SIMPLER algorithm both of which are explained in detail in Patankar[11].

Table 1. Values of ϕ, Γ and S of the Governing Equations

Equation	ϕ	Γ	S
x-directional momentum equation	v_x	μ	0
y-directional momentum equation	v_y	μ	$\frac{\rho_{ref} g\beta(h-h_{ref})}{c_p}$
energy equation	h	k/c_p	$-\frac{\partial(\rho\Delta H)}{\partial t}$

For a numerical solution of equations (1)-(4), the problem domain is covered by a set of rectangular control volume. The TDMA was used to solve the discretization equations. The TDMA is a very powerful and convenient equation slover for the linear algebraic equations. Numerical analyses are performed in a two-dimensional domain. The control volume and its grid in the x-y coordinate are shown in Fig. 3.

The power law scheme for the convection and diffusion terms is used to derive the discretization equation[11]. The fully implicit scheme in time is used to derive the discretization equation. We used the underrelaxation factor to speed up the iterative calculation and to avoid divergence. We applied 0.7 as a value of the relaxation factor. The flow chart for the SIMPLER algorithm is shown in Fig. 4.

The calculation domain is limited to the molten metal pool depicted in Fig. 5. The bottom surface boundary temperatures are varied from 253℃ to 266℃. The upper surface boundary condition is governed by the nucleate boiling heat transfer coefficient of the water. The heat transfer coefficients are varied as 15000, 20000 and 25000 W/m^{2}K for sensitivity analysis. Adiabatic boundary conditions are applied to the side walls.

In this calculation, if the enthalpy values are

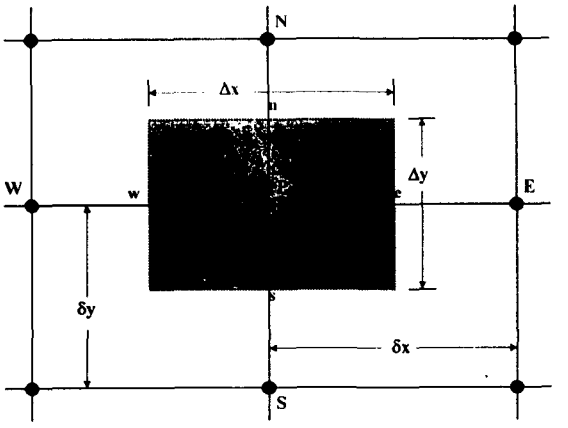

Fig. 3. Nodalization Scheme for Numerical Calculation

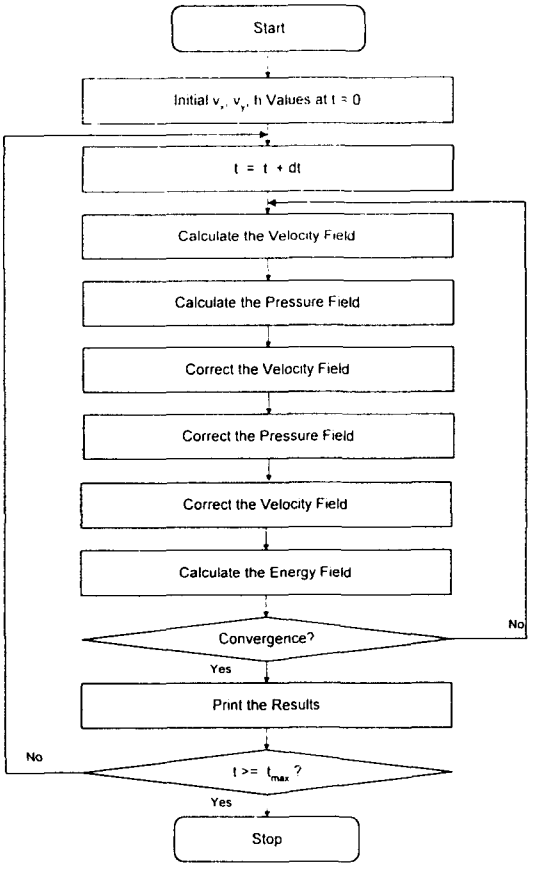

Fig. 4. Flow Chart for the SIMPLER Algorithm

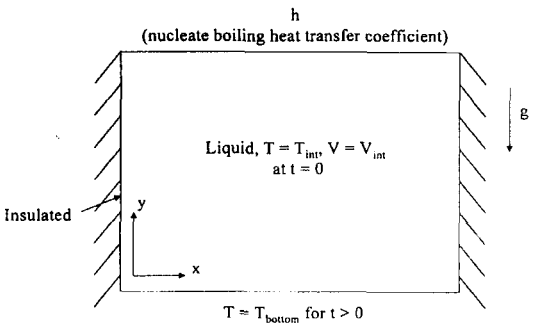

Fig. 5. Schematic Diagram for the Calculation Problem

varied within 10^{-3} from iteration to iteration, iterative calculation was considered to achieve the convergence criteria.

4. Results and Discussion

Fig. 6 shows the temperature distribution of the test section. Fig. 6(a) displays the temperature profile in the metal and coolant layers as a function of the coolant injection rate for a bottom heating temperature of 255℃. The portion below the horizontal dotted line is the metal layer, and thereabove is the coolant layer. The vertical dotted line is the melting temperature of tin. The temperature varies linearly in the solidified region, and is almost uniform in the molten pool and in the coolant. The crust thickness and temperature distribution are barely affected by the coolant injection rate. Figs. 6(b) displays the temperature profile for bottom heating surface temperatures of 253℃, 255℃, 258℃, 262℃ and 266℃ with the coolant injection rate of 1.5kg/min. The results illustrate that crust thickness and temperature of the metal layer are affected by the bottom surface temperature. As can be seen from Fig. 6(a) and 6(b), the crust layer thickness may be greatly varied by the heated bottom surface temperature of the test section, but is not much affected by the coolant injection rate as much as the current heat

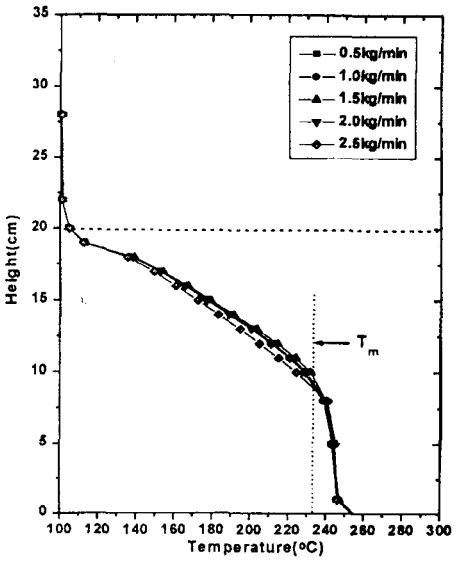

(a) Bottom Temperature : 255°C

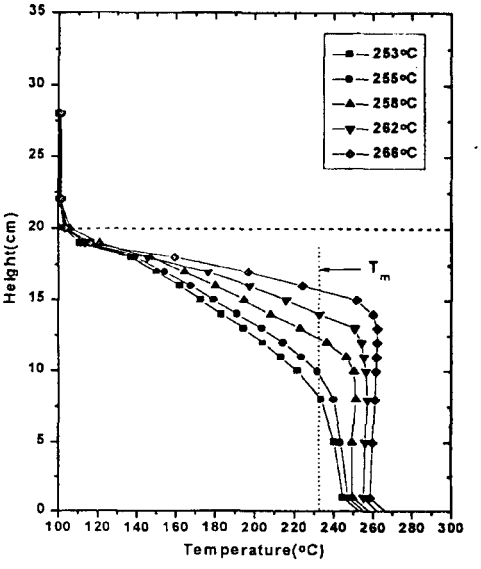

Fig. 6 Temperature Distribution in Metal Layer and Coolant

and coolant input rates are concerned.

Fig. 7 shows the numerical analysis results for (a)

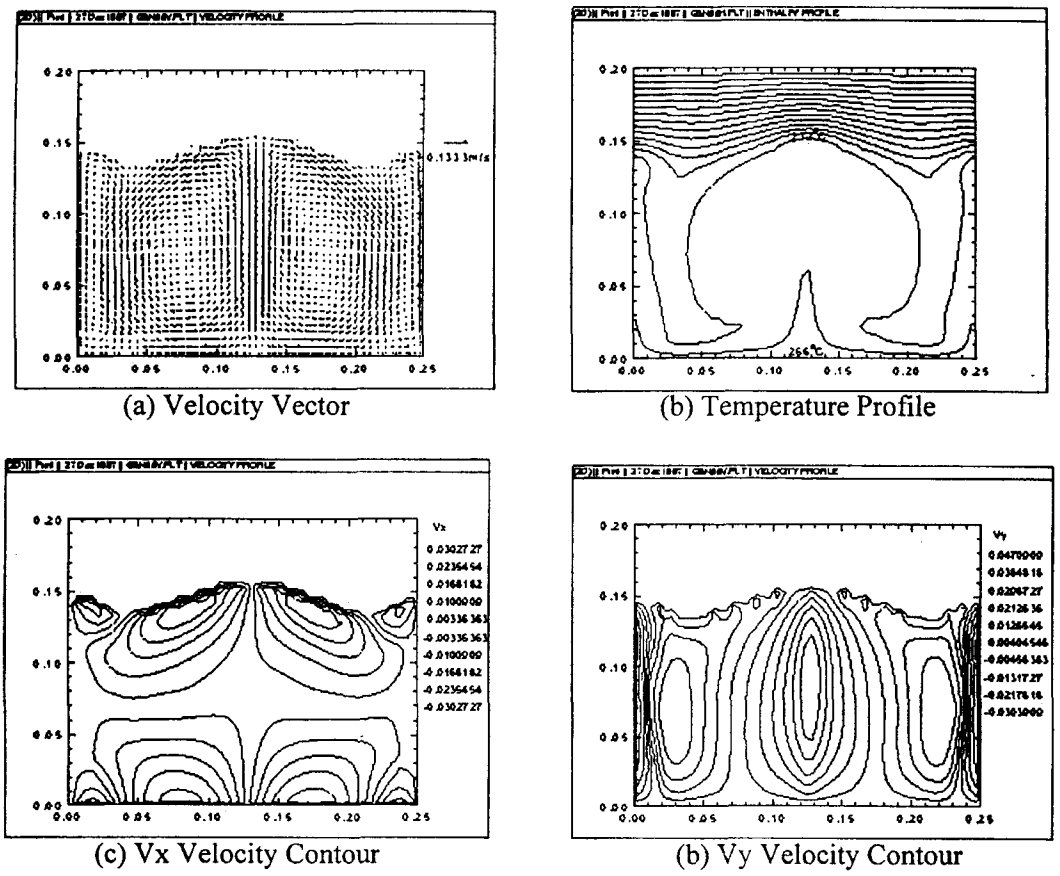

Fig. 7. Numerical Analysis Results of the Molten Metal Pool

the flow pattern, (b) the temperature distribution, and (c) the x-component and (d) the y-component velocity contours of the molten metal pool at quasi-steady state. The bottom heating temperature is 266 °C and the upper boundary condition is given by the nucleate boiling heat transfer coefficient of 20000 W/m^{2}K. Fig. 7(a) presents the molten pool flow pattern, with the empty area representing the solidified (crust) region. The arrow on the right side signifies the unit vector magnitude of 0.1333m/s. The temperature varies fairly linearly within this crust region as shown in Fig. 7(b). The x-component velocity, v_x, in Fig. 7(c), varies from 0.0303m/s (from left to right) to -0.0303m/s (from right to left), while the y-component velocity, v_y, in Fig. 7(d), changes from 0.0471m/s (upward) to -0.0304m/s (downward).

Table II presents a comparison of the experimental data and the numerical calculation results for the natural convection heat transfer rates and crust thickness in the molten metal layer. The values were obtained after a steady state had been accomplished. In actuality, the quasi-steady state apparently produced fluctuations in temperature in the metal layer and the coolant. The experimental data in Table II were obtained by time-averaging the measured values after the

quasi-steady state had been reached. In the calculation, the heat flux and the crust thickness are the average values of the x-directional nodes.

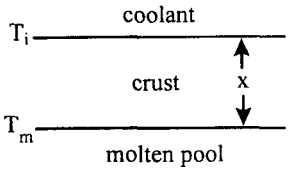

Fig. 8. Crust Layer and Interface Temperature of the Metal Pool

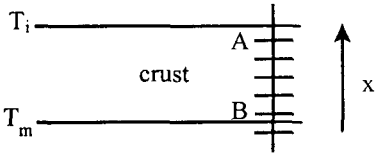

Fig. 9. Temperature Reading Locations for Heat Flux Calculation

In the test, the crust thickness is determined by the linear interpolation method from the thermocouple reading data and the melting temperature (232°C) for pure tin. The heat flux can be derived from the temperature difference between the top surface and the bottom surface of the crust layer as shown in Fig. 8 using the heat conduction equation.

$$q'' = k\frac{T_m - T_i}{x} \tag{8}$$

where

q″ : heat flux through crust

k : thermal conductivity of crust

T_i : interface temperature of crust and coolant

T_m : melting temperature

x : crust thickness

In this study, the actual heat flux was calculated from the temperature measurements by the thermocouples located right underneath the metal

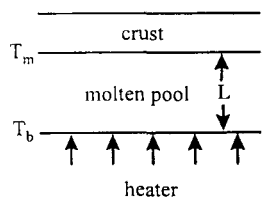

Fig. 10. Crust and Molten Pool in Metal Layer

layer and coolant interface and just above the melting point, and the distance between the two points in-between as shown in Fig. 9.

$$q'' = k\frac{T_B - T_A}{x_A - x_B} \tag{9}$$

This was necessary because the interfacial temperature T_i and the melting location of the metal layer normally fell between the two thermocouple locations.

The heat transfer coefficient of the molten metal pool is derived from this heat flux as follows.

$$h = \frac{q''}{T_b - T_m} \tag{10}$$

T_b and T_m are denoted in Fig. 10. This calculation is based on the assumption that there is no heat loss to the environment. Natural convection heat transfer in the molten pool is generated by the buoyancy force arising from the density difference. The Nu number and the Ra number are defined as follows.

$$Nu = \frac{hL}{k} \tag{11}$$

$$Ra = \frac{g\beta\Delta TL^3}{\alpha\nu} \tag{12}$$

where

h : heat transfer coefficient in the molten pool

L : height of molten pool layer

Table 2. Heat Transfer Rates of the Molten-Metal Pool

Bottom Temp. (C)	Crust Thickness (cm)				Heat Flux ($\times 10^4$ W/m^2)				Ra Number ($\times 10^6$)				Nu Number			
	Exp.	Cal. Upper Boundary Heat Trans. Coeff. ($\times 10^3$W/m^{2}K)			Exp.	Cal. Upper Boundary Heat Trans. Coeff. ($\times 10^3$W/m^{2}K)			Exp.	Cal. Upper Boundary Heat Trans. Coeff. ($\times 10^3$W/m^{2}K)			Exp.	Cal. Upper Boundary Heat Trans. Coeff. ($\times 10^3$W/m^{2}K)		
		15	20	25		15	20	25		15	20	25		15	20	25
253	11.1~12.8	11.59	11.77	11.83	5.97~6.21	6.81	6.76	6.76	1.62~3.50	2.55	2.40	2.35	7.1~8.0	9.5	9.3	9.2
255	10.0~10.9	9.42	9.50	9.54	7.47~7.89	8.14	8.17	8.15	3.54~5.01	5.85	5.72	5.65	10.2~11.2	12.5	12.4	12.4
258	7.6~7.8	7.99	8.14	8.18	9.39~9.60	9.84	9.74	9.77	10.1~11.1	9.68	9.32	9.23	14.5~15.0	15.2	14.8	14.8
262	5.3~6.0	6.47	6.94	7.00	14.4~14.5	11.93	11.54	11.57	20.6~27.8	16.0	14.4	14.2	20.5~23.8	17.9	16.8	16.7
266	3.7~4.3	5.09	5.29	5.37	16.9~18.4	14.64	14.43	15.05	22.4~35.5	24.2	23.3	22.9	20.2~24.8	21.4	20.8	20.6

ΔT : temperature difference (T_b - T_m)
g : gravitational acceleration
α : thermal diffusivity
β : thermal expansion coefficient
ν : kinematic viscosity

The experimental results for the heat transfer show general agreement with the calculation results. However, the experimental values are higher than the calculation results for high bottom surface temperatures. It is considered that this discrepancy results from the difference between the metal layer and coolant interface temperatures in computation and tests.

The relationship between the Nusselt number and the Rayleigh number in the molten metal pool region was determined and compared against the experimental data without coolant boiling, the dry experimental data without coolant or solidification of the molten metal pool, and the literature correlations. The experiment without coolant boiling was performed using a low temperature melting alloy consisting weight percentage of Bi(49.92%), Pb(26.93%), Sn(13.28%) and Cd(9.85%) with a melting temperature of 70℃. The bottom heating method was the same as in this work, but the cooling mechanism was subcooled coolant natural convection using a heat exchanger at the top of the test section[12-14]. Fig. 11 shows a comparison of the present experimental and numerical results with the experimental data without coolant boiling and other correlations in the molten metal pool region. The present experimental data are taken from different bottom surface temperatures of 253℃, 255℃, 258℃, 262℃ and 266℃, respectively. The numerical analysis results are obtained using a nucleate boiling heat transfer coefficient of 20000 W/m^{2}K. A great deal of experimental studies were performed on the Rayleigh-Benard problem which deals with natural convection heat transfer. Their results are generally presented in the following fit correlation:

$$Nu = aRa^b \tag{13}$$

Technological needs have led to a great deal of experimental work being devoted to obtaining heat transfer coefficients. Especially, many experimental studies have been

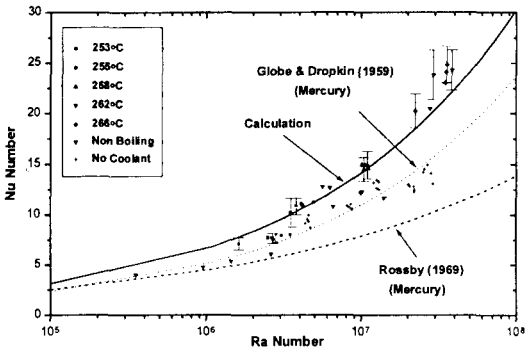

Fig. 11. Comparison of the Present Results with Literature Correlations

performed on the Rayleigh-Benard problem concerning natural convection in a horizontal layer, heated from below and cooled form above. In this problem, bottom or external heating of the layer induces the natural convection process. Experimental results have been reported by Globe and Dropkin[15], Rossby[16], Threfall[17], Heslot et al.[18], Chu and Goldstein[19], Garon and Goldstein[20], and Somerscales and Gazda[21]. Liquid metals, characterized by low Prandtl Numbers (0.01~0.1), often behave somewhat differently than water or gas. The mercury data of Globe and Dropkin[15] and of Rossby[16] represent the available data for liquid metal. However, these experiments were performed for a condition of one layer with pure mercury and without solidification by coolant layer.

$$\text{Globe and Dropkin} : Nu = 0.051 Ra^{0.333} \quad (14)$$

$$\text{Rossby} : Nu = 0.147 Ra^{0.247} \quad (15)$$

In this experiment, the heat transfer is accompanied by conjugate heat transfer mechanisms of the natural convection heat transfer in the molten metal pool, the conduction heat transfer in the solidified crust layer and the boiling heat transfer in the coolant layer. Especially, the molten metal layer is cooled by the rapid boiling heat transfer of the coolant. The present experimental results for heat transfer from the molten metal pool are higher than those without coolant boiling.

5. Conclusions

Experimental and numerical studies were performed to investigate the heat transfer characteristics and crust formation of a molten metal pool with natural convection concurrent with forced convective boiling of the overlying coolant. In the tests the temperature distribution and crust layer thickness in the metal layer were appreciably affected by the heated bottom surface temperature of the test section, but not much by the coolant injection rate. Numerical analyses were performed in the two-dimensional domain. The calculation domain was limited to the molten metal pool. The experimental results for heat transfer show general agreement with the calculation results. However, the experimental results are higher than the calculation results for high bottom surface temperatures.

In this experiment, the heat transfer is accompanied by solidification of the molten metal pool in the boiling coolant. The present experimental results for heat transfer on the molten metal pool are apparently higher than those without coolant boiling. This is probably because this experiment was performed with concurrent solidification of the molten metal pool and rapid boiling of the coolant. On the other hand, comparison experimental tests were performed without coolant boiling and the correlation was developed for the pure molten metal without coolant phase change. Note

however that the test results may not directly be applied to an actual reactor accident condition because this study was performed in a lower Ra number region than for the actual molten debris. During a severe accident, the molten debris may reach the 10^{15}~10^{16} range of Ra number for the oxide pool and the 10^{9}~10^{10} range for the metallic layer[22]. Further study is planned to investigate the effect of boiling coolant in the high temperature and high Rayleigh number region.

References

1. E. L. Tolman, P. Kuan and J. M. Broughton, "TMI-2 Accident Scenario Update," Nucl. Eng. & Des., 108, 45 (1988).
2. K. Y. Suh, "Modeling of Heat Transfer to Nuclear Steam Supply System Heat Sinks and Application to Severe Accident Sequences," Nucl. Tech., 106, 274 (1994).
3. K. Y. Suh and R. E. Henry, "Integral Analysis of Debris Material and Heat Transport in Reactor Vessel Lower Plenum," Nucl. Eng. Des., 151, 203 (1994).
4. K. Y. Suh and R. E. Henry, "Debris Interactions in Reactor Vessel Lower Plena During a Severe Accident: I. Predictive Model," Nucl. Eng. Des., 166, 147 (1996).
5. K. Y. Suh and R. E. Henry, "Debris Interactions in Reactor Vessel Lower Plena During a Severe Accident: II. Integral Analysis," Nucl. Eng. Des., 166, 165 (1996).
6. D. R. Bradley and D. R. Gardner, CORCON-MOD3 : An Integrated Computer Model for Analysis of Molten Core-Concrete Interactions, NUREG/CR-5843 (1992).
7. Jae-Seon Cho, "The effect of Boiling Coolant on Natural Convection Heat Transfer and Solidification of Liquid Metal Layer with High Temperature," Ph. D. Thesis, Seoul National University (1999).
8. R. J. Park et al., "A Study on Natural Convection Heat Transfer with Crust Formation in the Corium Pool," KAERI/TR-1322/99 (1999).
9. V. R. Voller and C. Prakash, "A Fixed Grid Numerical Modelling Methodology for Convection-Diffusion Mushy Region Phase-Change Problems," Int. J. Heat & Mass Trans., 30, 1709 (1987).
10. V. R. Voller, M. Cross and N. C. Markatos, "An Enthalpy Method for Convection/ Diffusion Phase Change," Int. J. Num. Meth. Eng., 24, 271 (1987).
11. S. V. Patankar, *Numerical Heat Transfer and Fluid Flow*, Hemisphere Publishing Corp., Washington D.C. USA (1980).
12. R. J. Park et al., "A Study on the Crust Formation of Molten Core Material without Coolant Boiling," KAERI/TR-466/94, (1994).
13. R. J. Park, S. B. Kim, H. D. Kim, and S. M. Choi, 1997, "Crust Formation and Its Effect on Heat Transfer in the Molten Metal Pool," International Meeting on Advanced Reactors Safety ARS97, pp. 81-88, Orlando, FL, USA, June (1997).
14. Rae-Joon Park, "Solidified Crust Formation and Its Effect on Heat Transfer between Horizontal Liquid Layers," Ph. D. Thesis, KAIST (1998).
15. S. Globe and D. Dropkin, "Natural Convection Heat Transfer in Liquid Confined by Two Horizontal Plates and Heated from Below," J. of Heat Transfer, 81, 24 (1959).
16. H. T. Rossby, "A Study of Benard Convection with and without Rotation," J. of Fluid Mech., 36, 309 (1969).
17. D. C. Threlfall, "Free Convection in Low-Temperature Gaseous Helium," J. of Fluid Mech., 67, 17 (1975).

18. F. Heslot, B. Castaing and A. Libchabre, "Transitions to Turbulence in Helium Gas," Phys. Rev., A36, 5870 (1987).
19. T. Y. Chu and R. J. Goldstein, "Turbulent Convection in a Horizontal Layer of Water," J. of Fluid Mech., 60, 141 (1973).
20. M. Garon and R. J. Goldstein, "Velocity and Heat Transfer Measurements in Thermal Convection," Phys. Fluids, 16, 1818 (1973).
21. E. F. C. Somerscales and I. W. Gazda, "Thermal Convection in High Prandtl Number Liquids at High Rayleigh Numbers," Rensselaer Polytechnic Institute, ME Report HT-5, Troy, NY, USA (1968).
22. T. G. Theofanous, *et al.*, In-Vessel Coolability and Retention of a Core Melt, DOE/ID-10460, July (1995).